Eur Biophys J (2011) 40:805–810
DOI 10.1007/s00249-011-0690-7

BIOPHYSICS LETTER

Imaging interactions of cationic antimicrobial peptides with model lipid monolayers using X-ray spectromicroscopy

Bonnie O. Leung · Adam P. Hitchcock · Amy Won · Anatoli Ianoul · Andreas Scholl

Received: 10 November 2010 / Revised: 11 February 2011 / Accepted: 16 February 2011 / Published online: 5 March 2011

Abstract The interaction of antimicrobial peptide anoplin with 1,2-dipalmitoyl-*sn*-glycero-3-[phospho-*rac*-(1-glycerol)] lipid monolayers was imaged with atomic force microscopy, scanning transmission X-ray microscopy, and X-ray photoemission electron microscopy. X-ray absorption spectromicroscopy of the surface revealed the domains of the phase-segregated surface to be composed of 98(±5)% lipid while the matrix consisted of a ~50:50 lipid-peptide mixture. We show X-ray spectromicroscopy to be a valuable quantitative tool for label-free imaging of lipid monolayers with antimicrobial peptides at a lateral spatial resolution below 80 nm.

Keywords Lipid · Membrane · Antimicrobial peptide · Anoplin · X-ray microscopy · X-PEEM · STXM

Introduction

Cationic antimicrobial peptides can insert into the negatively charged lipid membranes of Gram-negative and Gram-positive bacteria forming channels in the cytoplasmic membrane that result in lysis or leakage through the membrane barrier (Zhang et al. 2001; Hancock and Sahl 2006). The mechanism of peptide penetration into the bacterial membrane has been proposed to vary, depending on the peptide (Zhang et al. 2001), and include membrane phase separation, membrane thinning, and bilayer disruption (i.e., pore formation or carpeting of peptide over the lipid bilayer) (Habermann 1972).

The interactions between antimicrobial peptides and model bacterial cell membranes have been imaged by laser-scanning confocal microscopy (Park et al. 2000), scanning (Park et al. 2008) and transmission electron microscopy (Park et al. 2006), and atomic force microscopy (AFM) (Shaw et al. 2008). The main advantage of these studies is the direct visualization of the effect of peptide addition or adsorption to the lipid layer or cell wall. For example, an AFM study of indolicidin peptide addition to model lipid bilayers revealed a change in surface morphology (Shaw et al. 2008). The main disadvantage of these studies is the limited chemical information provided by these types of microscopies.

Synchrotron-based X-ray spectromicroscopy techniques such as scanning transmission X-ray microscopy (STXM) (Kilcoyne et al. 2003) and X-ray photoemission electron microscopy (X-PEEM) (Anders et al. 1999) are outstanding label-free tools for chemically and spatially mapping biological samples (Leung et al. 2010). For example, STXM has been used to map metals in biofilms (Hitchcock et al. 2009) and to study lipid vesicles (Nováková et al. 2008), while X-PEEM has been used to study protein and peptide adsorption to model biomaterials (Leung et al. 2009a, b; Leung et al. 2010). By analyzing the extracted near-edge X-ray absorption fine structure (NEXAFS) spectra of different spatial regions, complex biomolecules such as DNA, lipids,

Electronic supplementary material The online version of this article (doi:10.1007/s00249-011-0690-7) contains supplementary material, which is available to authorized users.

B. O. Leung · A. P. Hitchcock (✉)
Department of Chemistry and Chemical Biology, McMaster University, Hamilton, ON L8S 4M1, Canada
e-mail: aph@mcmaster.ca

A. Won · A. Ianoul
Department of Chemistry, Carleton University, Ottawa, ON K1S 5B6, Canada

A. Scholl
Advanced Light Source, Berkeley Lab, Berkeley, CA 94720, USA

proteins or peptides, and carbohydrates can be easily distinguished, identified, and quantitatively mapped.

In this study, we use NEXAFS spectromicroscopy to simultaneously identify both lipid and peptide without external markers and to quantify the percentages of lipid and peptide present in various regions of the sample. Furthermore, we examine lipid monolayers, which are more challenging due to the smaller amount of material present compared to lipid bilayers. Lipid monolayers are commonly used as model membranes and are considered to mimic the outer leaflet of the lipid bilayer (Erbe et al. 2009; Neville et al. 2010; Arseneault et al. 2010) even though they do not fully represent the true biological membrane, which includes membrane proteins, pumps, pH gradients, etc. (Hancock and Rozek 2002).

Experimental procedures

Anoplin (GLLKRIKTLL-OH) was synthesized by Gen Script (purity ≥98%). The peptide was dissolved in 0.01 M phosphate-buffered saline (PBS, 138 mM NaCl, 2.7 mM KCl, Sigma-Aldrich) and stored at −14°C. 1,2-Dipalmitoyl-*sn*-glycero-3-[phospho-*rac*-(1-glycerol)] (DPPG) was purchased from Avanti Polar Lipids and used as received.

Lipid monolayers were formed on a Langmuir-Blodgett (LB) trough (NIMA 311-D, Coventry, UK) in 200 ml of PBS. Lipid/peptide monolayers were obtained by spreading DPPG/anoplin mixture in 50/50 mol ratio at the air/water interface. The trough was equilibrated for 15 min for solvent evaporation and compressed at 5 cm^2/min for two isotherm cycles. The monolayer was compressed to 30 mN/m and transferred onto freshly cleaved mica (for AFM, 1 × 1″ Hi-Grade Mica, Ted Pella, Redding, CA), 1 × 1 cm^2 silicon wafer (for X-PEEM), or a 0.5 × 0.5 cm^2 Si_3N_4 window with the underside covered by foil (for STXM) at 1 mm/min, with transfer ratios greater than 80%. The reference spectra of anoplin and DPPG obtained via STXM were collected from samples (1 mg/ml) drop cast on a Si_3N_4 window.

All X-ray spectromicroscopy data were collected at the Advanced Light Source using the X-PEEM on beamline 7.3.1 (Anders et al. 1999) or the polymer STXM on beamline 5.3.2.2 (Kilcoyne et al. 2003). For X-PEEM, photoelectrons and secondary electrons ejected by absorption of 70–80% right circularly polarized monochromatic X-rays are accelerated into an electrostatic imaging column, where the spatial distribution is magnified and detected by a CCD camera. X-PEEM is a partial electron yield technique with a strong emphasis on low kinetic energy secondary electrons. Thus, X-PEEM is highly surface sensitive with a sampling depth (1/e) of 4 nm for polymers (Wang et al. 2009), with the integrated signal probing the top 10 nm of the sample. STXM and X-PEEM collect NEXAFS spectra in two different ways: STXM operates in transmission mode while X-PEEM uses a total electron yield detection method. Thus, STXM samples the entire film thickness, while X-PEEM typically detects the top 10 nm of a surface, which is the electron escape depth at the carbon edge.

Typically, for both X-PEEM and STXM, spectra are collected as sequences of 25–100 images, which are aligned post-acquisition (if needed) and, for STXM, are converted from transmission to optical density scale using the incident flux spectrum recorded from a clean area on the Si_3N_4 window. The spectrum at each pixel of the image sequence is then fitted with reference spectra by means of singular value decomposition (SVD) (Strang 1988; Koprinarov et al. 2002).

Since the reference spectra are set to an intensity response for 1 nm thickness of standard density of each material, the array of fit coefficients from fits of the STXM data to a set of chemical components (DPPG and anoplin) constitutes quantitative maps of the components. For X-PEEM the sum of the mapping signals is normalized such that the total thickness is 10 nm. In each case the quantitative analysis is verified by applying a threshold mask to each component map to isolate pixels corresponding to the lipid-rich or peptide-rich regions. The average NEXAFS spectrum in each region was extracted and fitted with a linear combination of either the lipid or peptide reference spectra.

Radiation damage was minimized by collecting the minimum number of energy images that could differentiate the species and by using short dwell times (X-PEEM 1s, STXM 1 ms). For X-PEEM, data were collected only on pristine areas not previously exposed to the X-ray beam. For STXM, an image was collected after each stack at a damage sensitive energy to verify that the extent of damage was negligible. We have previously quantified radiation damage rates in both X-PEEM and STXM for highly radiation-sensitive polymers such as poly(methyl methacrylate) (PMMA) (Wang et al. 2009). Although, we have not quantified the dose-damage relationship for lipids, qualitatively the damage rate for lipids is slower than that for PMMA, while the acquisition methods we used are suitable to study PMMA.

The atomic force microscopy (AFM) images were collected with an Ntegra (NTMDT, Russia) microscope in semi-contact mode operated in air. Cantilevers with rotated monolithic silicon tips (125 μm long, 40 N/m spring constant Tap 300 Al, resonance frequency 315 kHz, Budget Sensors) were used with a scan rate of 0.5 Hz.

Results and discussion

As shown previously (Hitchcock et al. 2009), the NEXAFS spectra of lipids and proteins are easily distinguishable. The

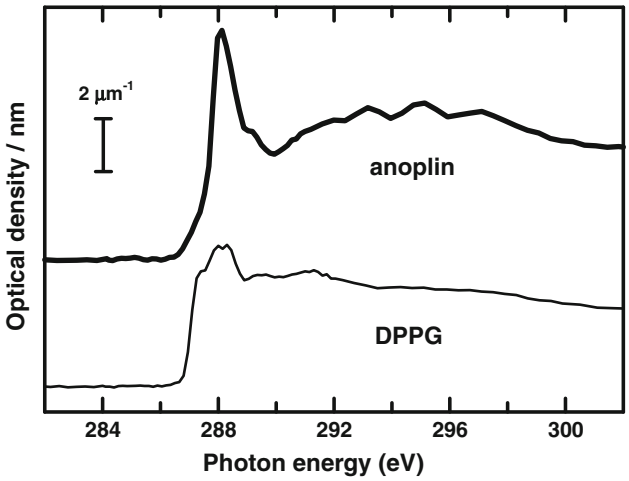

Fig. 1 C 1s X-ray absorption spectra of DPPG (*thin line*) and anoplin (*thick line*) as recorded in STXM. The spectra are plotted on an absolute linear absorbance scale, after subtraction of a linear background to isolate only the C 1s signal. Offset used for clarity

same techniques can be applied to peptide interactions with model lipids to elucidate information on the mechanisms of antimicrobial peptide activity. Herein, we report the STXM and X-PEEM mapping of an antimicrobial peptide (anoplin, GLLKRIKTLL-OH) incorporated into a lipid monolayer.

The NEXAFS reference spectra of pure DPPG and anoplin as obtained via STXM are shown in Fig. 1. The NEXAFS spectrum of anoplin is dominated by an intense transition at 288.2 eV, corresponding to the C 1s $\rightarrow \pi^*_{C=O}$ transition of the peptide amide backbone. Compared to other biomolecules such as human serum albumin (HSA) protein or the arginine-rich cationic peptide SUB-6 (Leung 2009a, b; Stewart-Ornstein et al. 2007; Leung et al. 2008), the amino acid sequence of anoplin does not contain aromatic residues, and thus there is no C 1s $\rightarrow \pi^*_{C=C}$ transition at 285.2 eV, which only exists if there are carbon–carbon double bonds.

The NEXAFS reference spectrum of DPPG lipid is slightly more complex with two intense transitions at 288.05 and 288.32 eV and a shoulder at 287.45 eV. The transition at 288.32 eV is assigned as the C 1s $\rightarrow \pi^*_{C=O}$ transition, which is similar to the position of the corresponding transition in the NEXAFS spectra of other lipids such as 1,2-dioleoyl-sn-glycero-3-phosphatidylserine (DOPS) (Wang et al. 2009; Peth et al. 2009) or 1,2-dioleoyl-sn-glycero-3-phosphatidyl-choline (DOPC) (Nováková et al. 2008). The transitions at 287.45 and 288.01 eV are tentatively assigned as C 1s $\rightarrow \sigma^*_{C-H}$. This assignment is based on the NEXAFS spectrum of hexacontane, a saturated alkane that greatly resembles the hydrophobic tail of the DPPG lipid.

The NEXAFS spectrum of pure hexacontane has two C 1s $\rightarrow \sigma^*_{C-H}$ transitions at 287.63 and 288.23 eV (Fu and Urquhart 2005). Furthermore, hexacontane has been shown to exhibit strong linear dichroism, with the two C 1s $\rightarrow \sigma^*_{C-H}$ transitions being the most intense and weakest (almost zero) when the electric field vector of the X-ray is aligned parallel or perpendicular to the C–H orbitals, respectively (Fu and Urquhart 2005). At intermediate angles (e.g., 50°), the transition at 287.6 eV is only seen as a shoulder (Fu and Urquhart 2005). Since our lipid reference sample was drop-cast onto the silicon nitride X-ray transparent substrate, the chains should be randomly oriented, giving rise to the observed shoulder at 287.5 eV for the lipid sample.

DPPG and anoplin are easily distinguished from each other using NEXAFS. Firstly, DPPG exhibits a shoulder at 287.5 eV, which is not present in the anoplin NEXAFS spectrum, and secondly, the spectral line shape of anoplin is narrow since it only has one transition around ~288 eV, while the lineshape of DPPG is wide (~2 eV) due to the presence of three transitions around 288 eV.

Figure 2 presents an example of mapping of DPPG:anoplin 50:50 in this system by X-PEEM. Pixels rich in lipid (Fig. 2a) or peptide (Fig. 2b) are isolated, and the average NEXAFS spectrum of the lipid-rich (Fig. 2c, dots) or peptide-rich (Fig. 2d, dots) areas is extracted from these regions. Next, the average NEXAFS spectrum is fitted with the reference spectra of pure DPPG lipid or pure anoplin peptide via least squares refinement to obtain the best fit and also the quantitative results.

Figure 3 presents comparative AFM, STXM, and X-PEEM micrographs of a 50% mole ratio DPPG/anoplin monolayer. The AFM image shows large domains and small domains that are >10 μm and ~500 nm across, respectively (Fig. 3a). The mean total film thickness is approximately 2.5 nm. While AFM shows excellent spatial resolution, it has poor chemical sensitivity for distinguishing whether the domains are composed of pure lipid or a lipid/peptide mix.

In contrast, X-ray spectromicroscopy techniques provide outstanding chemical detection with good spatial resolution (30–80 nm). Figure 3b, c displays the STXM component maps for DPPG and anoplin, respectively, and Fig. 3d shows the color-coded maps with DPPG coded in red and anoplin coded in green. The maps illustrate that the films are composed primarily of lipid or peptide domains. However, the NEXAFS spectra extracted from the lipid-rich or peptide-rich domains are noisy due to the thinness in the layer, and some radiation damage is apparent in the peptide spectrum with double-bond formation shown by the transitions arising at ~285 eV (Fig. 1 in the Electronic supplementary material).

STXM operates in transmission mode (log I_0/I) and typically requires a film thickness of ~100 nm to obtain the optimal optical density. For thin films that are only 2.5 nm thick, the transmitted intensity (I) is similar to the incident intensity (I_0) resulting in a weak absorption signal. However,

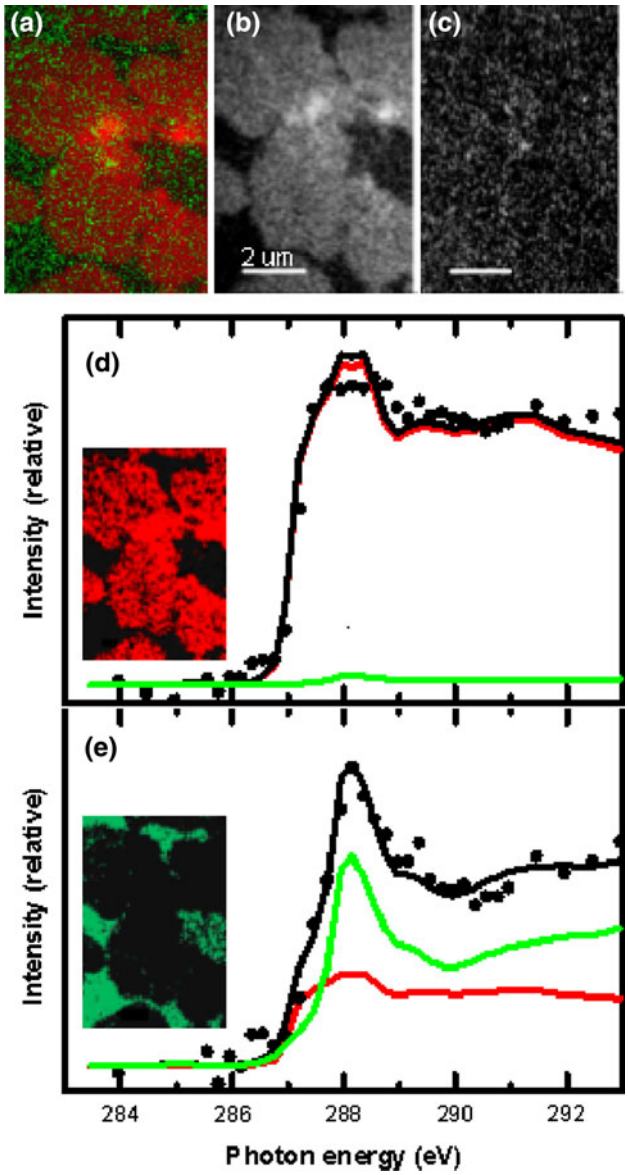

Fig. 2a–e X-PEEM-derived maps and spectra from anoplin interacted with a DPPG monolayer in a 1:1 mol ratio. **a** Rescaled color composite of the component maps for **b** DPPG (*red in composite*) and **c** anoplin (*green in composite*). Curve fit of the average C 1s spectra extracted from the **d** DPPG-rich areas and **e** anoplin-rich areas (data, *dots*; fit, *black line*; DPPG, *red*; anoplin, *green*). The inserts in **d** and **e** show pixels selected

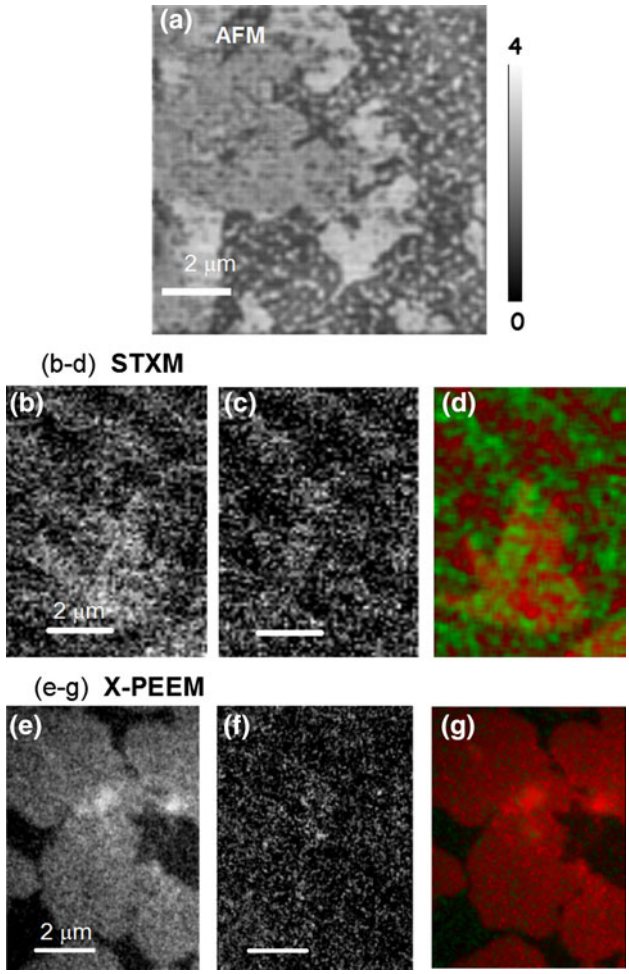

Fig. 3 **a** AFM image of DPPG and anoplin obtained via Langmuir-Blodgett. STXM component maps of **b** DPPG and **c** anoplin derived from C 1s image sequences and **d** absolute color composite map with DPPG and anoplin color-coded in *red* and *green*, respectively. X-PEEM component maps of **e** DPPG and **f** anoplin derived from C 1s image sequences and **g** the absolute color composite (same color scheme as **d**)

NEXAFS spectra can also be collected in total electron yield (TEY) mode with an X-PEEM. Since X-PEEM typically detects the top 10 nm of a film surface, X-PEEM is much more sensitive than STXM for analyzing these thin films.

Figure 3e–f displays the component maps of the DPPG and anoplin monolayers obtained from X-PEEM, and Fig. 3g shows the color composite map of DPPG and anoplin color-coded in red and green, respectively. The data quality obtained from X-PEEM for these thin films is improved compared to STXM. The X-PEEM composite map clearly shows that the large lipid domains are composed mainly of lipid while the matrix is dominated by peptide.

Quantitative results were obtained by extracting the average NEXAFS spectrum from either the DPPG-rich or peptide-rich regions of the stack and then fitting the experimental NEXAFS spectrum with the pure reference spectra. The extracted experimental spectra from X-PEEM are much less noisy compared to the spectra obtained from STXM. There is a slight dip at ~285 eV that results from carbon contamination of the X-PEEM beamline. The spectrum also demonstrates that X-PEEM is less damaging for thin films since there is a lack of double bond formation at ~285 eV. Most importantly, the spectroscopy obtained from the DPPG-rich and peptide-rich areas clearly shows different spectral line shapes, which can easily distinguish lipid from peptide. Furthermore, the fitting procedure

reveals the DPPG-rich areas to be composed mostly of lipid 98(±5)% while the peptide-rich regions are composed of ~50(±5)% lipid.

The spatial resolution of X-PEEM is projected to improve over the next few years with the implementation of aberration-corrected X-PEEMs (spatial resolution below 10 nm), which may allow detection and characterization of the pores created by many antimicrobial peptides that are on the order of several nanometers (Ladokhin et al. 1997; Bechinger 1999). Future STXM studies will study anoplin interactions with hydrated lipid bilayer membranes, since it is known that lipid films can rearrange when removed from aqueous solution.

To our knowledge, this is the first study using X-ray spectromicroscopy techniques to probe the interactions of antimicrobial peptides with lipid monolayers that model the outer surface of bacterial membranes. We have shown that by using X-PEEM, label-free and quantitative mapping of lipid and peptide is possible with a lateral spatial resolution below 80 nm. Our future studies aim to look at the more realistic peptide:lipid concentrations relevant to antimicrobial action (i.e., peptide:lipid 1:100), to use lipid bilayers, and to use STXM to carry out these studies in a fully hydrated system to be closer to real biological membranes.

Conclusions

NEXAFS spectromicroscopy and AFM techniques were used to imaging the interaction of antimicrobial peptide anoplin with DPPG lipid monolayers. X-PEEM quantification of the phase-segregated surface revealed the domains to be composed of almost 100% lipid, while the matrix was a 50:50 lipid:peptide mix. Our results show that X-PEEM can be used to image and quantify the interactions of antimicrobial peptides with lipid monolayers.

Acknowledgments This research is supported by the Natural Science and Engineering Research Council (NSERC), Early Researcher Award (ERA), Canadian Foundation for Innovation (CFI). X-ray microscopy was carried out using the polymer STXM and magnetic X-PEEM at the ALS, which is supported by the US DoE under contract DE-AC03-76SF00098. We thank David Kilcoyne, Tolek Tyliszczak, and Andrew Doran for their diligence and expertise in keeping the beamlines and microscopes in top condition.

References

Anders S, Padmore HA, Duarte RM, Renner T, Stammler T, Scholl A, Scheinfein MR, Stohr J, Seve L, Sinkovic B (1999) Photoemission electron microscope for the study of magnetic materials. Rev Sci Instrum 70:3973–3982

Arseneault M, Bedard S, Boulet-Audet B, Pezolet M (2010) Study of the interaction of lactoferricin b with phospholipid monolayers and bilayers. Langmuir 26:3468–3478

Bechinger B (1999) The structure, dynamics and orientation of antimicrobial peptides in membranes by multidimensional solid-state NMR spectroscopy. Biochim Biophys Acta 1462:157–183

Erbe A, Kerth A, Dathe M, Blume A (2009) Interactions of KLA amphipathic model peptides with lipid monolayers. Chem Bio Chem 10:2884–2892

Fu J, Urquhart SG (2005) Linear dichroism in the X-ray absorption spectra of linear n-alkanes. J Phys Chem A 109:11724–11732

Habermann E (1972) Bees and wasp venom. Science 177:314–322

Hancock REW, Rozek A (2002) Role of membranes in the activities of antimicrobial cationic peptides. FEMS Microbiol Lett 206:143–149

Hancock REW, Sahl HG (2006) Antimicrobial and host-defense peptides as new anti-infective therapeutic strategies. Nature Biotech 24:1551–1557

Hitchcock AP, Dynes JJ, Lawrence JR, Obst M, Swerhone GDW, Korber DR, Leppard GG (2009) Soft X-ray spectromicroscopy of nickel sorption in a natural river biofilm. Geobiology 7:432–453

Kilcoyne ALD, Tylisczak T, Steele WF, Fakra S, Hitchcock P, Franck K, Anderson E, Harteneck B, Rightor EG, Mitchell GE, Hitchcock AP, Yang L, Warwick T, Ade H (2003) Interferometer-controlled scanning transmission X-ray microscopes at the advanced light source. J Synchrotron Rad 10:125–136

Koprinarov IN, Hitchcock AP, McCrory CT, Childs RF (2002) Quantitative mapping of structured polymeric systems using singular value decomposition analysis of soft X-ray images. J Phys Chem B 106:5358–5364

Ladokhin AS, Selsted ME, White SH (1997) Sizing membrane pores in lipid vesicles by leakage of co-encapsulated markers: pore formation by melittin. Biophysical J 72:1762–1766

Leung BO, Hitchcock AP, Brash JL, Scholl A, Doran A, Henklein P, Overhage J, Hilpert K, Hale JD, Hancock REW (2008) An X-ray spectromicroscopy study of competitive adsorption of protein and peptide onto polystyrene-poly(methyl methacrylate). Biointerphases 3:F27–F35

Leung BO, Hitchcock AP, Cornelius R, Brash JL, Doran A, Scholl A (2009a) An X-ray spectromicroscopy study of protein adsorption to a polystyrene-polylactide blend. Biomacromolecules 10:1838–1845

Leung BO, Wang J, Brash JL, Hitchcock AP (2009b) Imaging hydrated albumin on a polystyrene-poly(methyl methacrylate) blend surface with X-ray spectromicroscopy. Langmuir 25:13332–13335

Leung BO, Brash JL, Hitchcock AP (2010) Characterization of biomaterials by soft X-ray spectromicroscopy. Materials 3:3911–3938

Neville F, Ivankin A, Konovalov O, Gildalevitz D (2010) A comparative study on the interactions of SMAP-29 with lipid monolayers. Biochim Biophys Acta 1798:851–860

Nováková E, Mitrea G, Peth C, Thieme J, Mann K, Salditt T (2008) Solid supported multicomponent lipid membranes studied by X-ray spectromicroscopy. Biointerphases 3:FB44–FB54

Park CB, Yi KS, Matsuzaki K, Kim MS, Kim SC (2000) Structure-activity analysis of buforin II, a histone H2A-derived antimicrobial peptide: the proline hinge is responsible for the cell-penetrating ability of buforin II. Proc Natl Acad Sci USA 97:8245–8250

Park SC, Kim JY, Shin SO, Jeong CY, Kim MH, Shin SY, Cheong GW, Park Y, Hahm KS (2006) Investigation of toroidal pore and oligomerization by melittin using transmission electron microscopy. Biochem Biophys Res Comm 343:222–228

Park SC, Kim MH, Hossain MA, Shin SY, Kim Y, Stella L, Wade JD, Park Y, Hahm KS (2008) Amphipathic α-helical peptide, HP (2–20), and its analogues derived from *Helicobacter pylori*: pore formation mechanism in various lipid compositions. Biochim Biophys Acta 1778:229–241

Peth C, Barkusky F, Sedlmair J, Gleber SC, Novakova E, Neimeyer J, Thieme J, Salditt T, Mann K (2009) Near-edge X-ray absorption fine

structure measurements using a laser plasma XUV source. J Phys Conf Ser 186:012032. doi:10.1088/1742-6596/186/1/012032

Shaw JE, Epand RF, Hsu JCY, Mo GCH, Epand RM, Yip CM (2008) Cationic peptide-induced remodelling of model membranes: direct visualization by in situ atomic force microscopy. J Struct Biology 162:121–138

Stewart-Ornstein J, Hitchcock AP, Hernàndez-Cruz D, Henklein P, Overhage J, Hilpert K, Hale J, Hancock REW (2007) Using intrinsic X-ray absorption spectral differences to identify and map peptides and proteins. J Phys Chem B 111:7691–7699

Strang G (1988) Linear algebra and its applications. Harcourt Brace Jovanovich, San Diego

Wang J, Morin C, Li L, Hitchcock AP, Zhang X, Araki T, Doran A, Scholl A (2009) Radiation damage in soft X-ray microscopy. J Electron Spectrosc Rel Phenom 170:25–36

Zhang L, Rozek A, Hancock REW (2001) Interaction of cationic antimicrobial peptides with model membranes. J Biol Chem 276: 35714–35722